Open Access

Dialectical Observation of Controllable Electrodeposited Ni Nanocones: the Unification of Local Disorder and Overall Order

Ruiqing Zou[1], Saidi Xiang[2], Jian Wang[1*], Yuhe Li[1], Lin Gu[1*] and Yanyan Wang[3]

Abstract

Dense and ordered Ni nanocones with regular spiral textures had been successfully synthesized via a simple and inexpensive electrodeposition process in the solution containing sodium chloride (NaCl), nickel chloride hexahydrate ($NiCl_2 \cdot 6H_2O$), and boric acid (H_3BO_3). After analyzing the microstructure, a more optimized possible growth mechanism of Ni nanocones was proposed, in which the growth process was divided into local and global aspects, named multi-dimensional growth mechanism of global order and local disorder. In an area small enough, any subtle state changes would cause disorder of Ni atom arrangement, which made the local microstructure appear disordered, but from a macro perspective, the difference between two adjacent disorders caused by different statuses was too small to be well reflected, only when the difference in state was large enough can the change be observed in the macroscopic appearance, so the global was orderly. Meanwhile, we found that the microstructure of Ni nanocones would be controlled in the electrodeposition solution by adjusting the experiment parameters such as the concentration of NaCl, $NiCl_2 \cdot 6H_2O$, and H_3BO_3, which indirectly determined the microstructure in a large extent via controlling the generation of intermediate products and the pH.

Keywords: Ni nanocones, Growth mechanism, Electrodeposition, Crystal modifier

Introduction

Nanostructured metals with unique surfaces [1] were widely used in a variety of fields, such as surface modification [2], ultra-hydrophobic layers [3–5], supercapacitors [6], microelectronic interconnection [7], nanoprobes [8], solar cells [9], gas sensors [10, 11], catalysts [12–19], mechanical polishing slurries [20], diamond wheels [21], nanoscale precision surfaces [22, 23]. As a result, many preparation techniques of nanostructured metal surfaces had been proposed, including hydrothermal method [10, 11], sol-gel method [24], template method [25], chemical vapor deposition method [26], chemical reduction method [27], and microemulsion method [28]. However, these traditional methods required a great deal of cost and time [2, 29].

In order to overcome the defects of traditional preparation methods mentioned above, electrodeposition technology has attracted significant research interest and has experienced magnificent developments. It would achieve the target expectation even under the milder conditions for the electric field could increase the reaction rate [2]. The preparation of electrodeposited nanostructured metal surfaces did not require complex auxiliary equipment, which greatly reduced the cost and time. Therefore, a great deal of research had been done on the preparation technology and formation mechanism of nanostructured metal surface topography via electrodeposition [30].

* Correspondence: wangjianxhu@163.com; gulinangle.222@163.com
[1]School of Materials Science and Engineering, Xihua University, Chengdu 610039, People's Republic of China
Full list of author information is available at the end of the article

In the specific electrodeposition preparation of nano-structured metal surface, the most representative method was the crystal modifier method [31]. The addition of crystal modifiers could affect the growth direction of crystals, so when reacted with an electrodeposition solution containing a specific crystal modifier, the metal nanostructured surface would grow in a specific direction. Therefore, the use of crystal modifier could easily obtain a specific, close-spaced, and regular 3D nanostructure on the surface of the metal substrate [32].

When a certain amount of ammonium chloride (NH_4Cl), which was the most used crystal modifier, was added to Ni electrodeposition solution, the NH_4^+ would form complex ions with Ni^{2+} and cause the electrodeposited Ni crystal to grow along (111) crystal face. Therefore, by adding NH_4Cl, it was easy to electrodeposit Ni nanocones that grow in a specific direction on the substrate metal surface and explain this phenomenon more accurately according to the growth mechanism of screw dislocation [33]. Furthermore, nickel, as a good ferromagnetic conductive metal, had the advantages of low price, wide use, and excellent corrosion resistance [34]. Ni nanocones obtained by electrodeposition with solution containing NH_4Cl had important applications in gas-sensitive sensors [10, 11], ultra-hydrophobic surfaces [3–5], and catalysts [12–19].

In this work, we replaced NH_4Cl with NaCl as the crystal modifier and prepared Ni nanocones successfully. Compared with NH_4Cl, NaCl was non-toxic, gentle, and stable. In addition, we put forward the possible specific complex structure and its role in the process of electrodeposition by combining hybrid orbital theory, molecular orbit theory, and actual characterization results. The growth mechanism of Ni nanocones electrodeposited in the solution containing NaCl, which was quite different from common screw dislocation-driven crystal growth mechanism [35], was expounded, and the effects of electrodeposition time and the concentration of NaCl, $NiCl_2$, and H_3BO_3 on the nanostructure of Ni nanocones were analyzed. Through the analysis of factors affected by the nanostructure of Ni nanocones, the controlled preparation was preliminarily realized, which would be instructive for the preparation of other special-shaped Ni nanocones in the future.

Materials and Methods
Materials
All chemical reagents were analytical pure and could be used directly for chemical reactions. The length, width, and thickness of Ni tablets (cathode and anode) used in our experiment were 70 mm, 25 mm, and 0.08 mm, respectively. Sodium chloride (NaCl), nickel chloride hexahydrate ($NiCl_2 \cdot 6H_2O$), boric acid (H_3BO_3), hydrochloric acid (HCl), and anhydrous ethanol (CH_3CH_2OH) were purchased from ChengDu Chron Chemicals Co., Ltd., China.

Surface Treatment and Sample Preparation
In a standard process, two Ni tablets (cathode and anode) were ultrasonically cleaned in deionized water and ethanol, respectively. The cathode Ni tablet was roughened in HCl (25 wt.%, 60 °C) for 30 min. Subsequently, Ni nanocones were electrodeposited on the as-prepared Ni tablets (cathode) from an aqueous solution containing $NiCl_2 \cdot 6H_2O$ (200 g/L), NaCl (100 g/L), and H_3BO_3 (50 g/L). The temperature (60 °C), current density (0.1 A), and electrodeposition time (20 min) should be regulated and another Ni tablet was employed as the anode to provide Ni ions (Ni^{2+}). After the electrodeposition, the cathode was ultrasonically cleaned in deionized water and then ethanol and finally dried in oven for 30 min, respectively. For further comparison, the electrodeposition time was controlled from 5 min to 50 min, and the concentration of NaCl, $NiCl_2 \cdot 6H_2O$, and H_3BO_3 was changed from 0 to 167 g/L, 0 to 400 g/L, and 0 to 50 g/L, respectively (Table 1).

Characterization
The scanning electron microscope (SEM) images and corresponding energy dispersive spectroscopy (EDS) were obtained through FEI Inspect F50 (Thermo Fisher, USA) operating at 20 kV. The X-Ray diffraction (XRD) patterns were measured using a D8 advance (BRUKER, Germany) X-ray diffractometer with a Cu Kα radiation (λ = 1.5406 Å). The Fourier Transform infrared spectroscopy (FTIR) pattern was measured using a Nicolet iS 10 (Thermo Fisher, USA) with an ATR module.

Results and Discussion
Determination of Intermediate Products
Usually, when NH_4Cl was used as crystal modifier, the NH_4^+ would form complex ions with the Ni^{2+} during the electrodeposition process [36]. Therefore, when NaCl was used as a crystal modifier, the solution might produce complex ions, which could promote the conduct of electrodeposition. Figure 1 shows the XRD patterns of electrodeposition solution which were heated and dried with an alcohol lamp (Fig. 1a) and with an oven (60 °C) (Fig. 1b), respectively, and the FTIR pattern of electrodeposition solution (Fig. 1c) after electrodeposition. We could see five different peaks clearly in Fig. 1a, which were NaCl (111), (200), (220), (222), and (400), respectively, compared with XRD standard PDF card. This indicated that the chemical bonds of the target product had been broken after the electrodeposition solution treated at high temperatures (alcohol lamp), in other words, the target product was resistant to poor high-temperature performance. Afterwards, we heated and dried the electrodeposition solution at a lower temperature (60 °C, oven), and the resulting XRD pattern was shown in Fig. 1b. Unfortunately, compared to

Table 1 Values of NaCl, NiCl₂·6H₂O, and H₃BO₃ concentration and electrodeposition time of different samples

Sample	Electrodeposition time (min)	NaCl concentration (g/L)	NiCl₂·6H₂O concentration (g/L)	H₃BO₃ concentration (g/L)
Ni_{355}	5	100	200	50
Ni_{370}	20	100	200	50
Ni_{400}	50	100	200	50
Ni_{270}	20	0	200	50
Ni_{437}	20	167	200	50
Ni_{170}	20	100	0	50
Ni_{570}	20	100	400	50
Ni_{320}	20	100	200	0
Ni_{345}	20	100	200	25

the XRD standard PDF cards for all possible compounds, nothing would correspond to these peaks. This suggested that the resulting target product was not a common general compound and might be a rare and special complex. Figure 1c shows the FTIR pattern of electrodeposition solution after electrodeposition, where we could find a peak around $1500 \, cm^{-1}$, which was consistent with the characteristic peak ($1499 \, cm^{-1}$) that the ionic liquid containing Ni halide anion had [37]. Therefore, combined with XRD and FTIR patterns, we considered that some complex ions ($[Ni_xCl_y]^{z-}$), which still presented after the reaction and had poor high-temperature resistance, were generated in the solution during the electrodeposition process.

When Cl^- encountered Ni^{2+} in the solution, Ni^{2+} would be hybridized according to the hybrid orbital theory and form $[Ni(H_2O)_2]Cl_4$. According to Fernandes et al., when the temperature was above 30 °C, the water molecules would be replaced by Cl^-. According to molecular orbital theory, each lone pair of Cl^- did not occupy a single orbit but divided all four orbits equally, the transition from an octahedral complex to a tetrahedral complex occurred [38]. Thus, each lone pair was consistent in both number and energy of occupied orbits, and

in theory, the resulting $[NiCl_4]^{2-}$ presented a structure of regular tetrahedron in space.

Effect of Electrodeposition Time and Crystal Modifier

Figure 2 shows low (Fig. 2 a_1–c_1) and high (Fig. 2a_2–c_2) magnification SEM images of Ni_{355}/Ni_{370}/Ni_{400} nanocones with different electrodeposition time (5 min, 20 min, 50 min) , XRD and EDS (Fig. 2 b_3, b_4) patterns of typical Ni_{370} nanocones (Fig. 2b_1), respectively. It was clear from SEM images that the cathode surface was covered by small and dense plate-like structure through a short electrodeposition time (5 min), and nanocone structures were gradually formed with the increase of electrodeposition time (20 min). With nanocones grown further, the sharp corners were clearer and more textures for longer periods of electrodeposition time (50 min). It was clear from the XRD pattern that there were three different diffraction peaks and all of them were consistent with pure Ni phase with face center cubic (fcc) structure, and no other impurity peaks such as NiO or $Ni(OH)_2$ could be detected. Meanwhile, it was obvious that Ni mainly grew along (220) crystal face. As can be seen from the EDS pattern of typical Ni_{370} nanocones, only Au and Ni could be confirmed, indicating
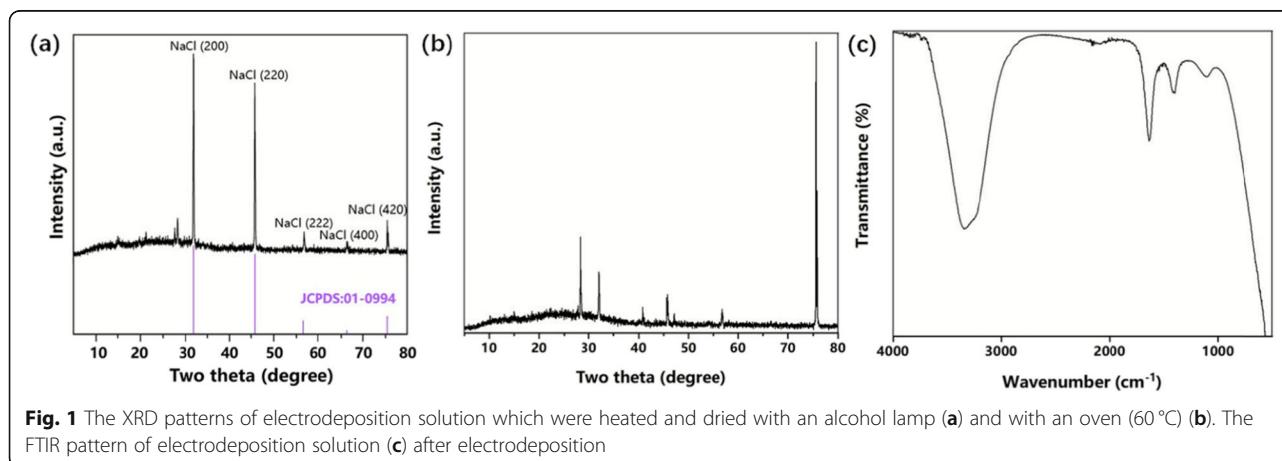

Fig. 1 The XRD patterns of electrodeposition solution which were heated and dried with an alcohol lamp (**a**) and with an oven (60 °C) (**b**). The FTIR pattern of electrodeposition solution (**c**) after electrodeposition
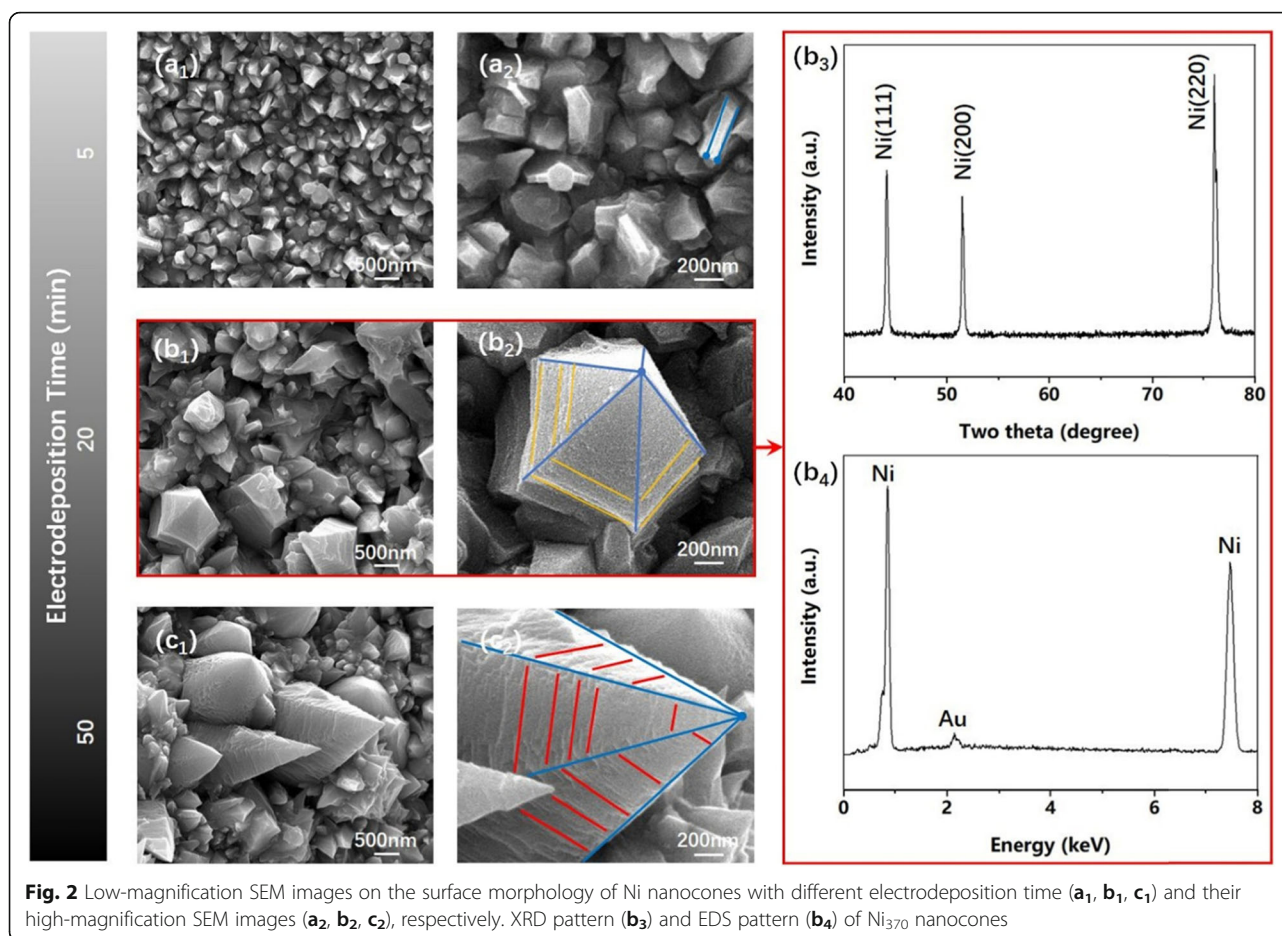
Fig. 2 Low-magnification SEM images on the surface morphology of Ni nanocones with different electrodeposition time (a_1, b_1, c_1) and their high-magnification SEM images (a_2, b_2, c_2), respectively. XRD pattern (b_3) and EDS pattern (b_4) of Ni_{370} nanocones

that what electrodeposited on the cathode was pure Ni_{370} nanocones without any contamination (Ni was a magnetic material, in order to attenuate magnetically and protect the probe, it needed to be sprayed with gold during SEM characterization).

Figure 3 shows the specific growth mechanism of Ni_{370} nanocones, named multi-dimensional growth mechanism of global order and local disorder. At the beginning, $[NiCl_4]^{2-}$ in the solution moved towards cathode under the action of electric field, Cl^- with negative electricality in the $[NiCl_4]^{2-}$ produced repulsive force against electrons on the cathode, whereas Ni^{2+} with positive electricality were attracted to the cathode after entering the diffusion layer. Both repulsive and attractive forces increased significantly, after entering the Helmholtz double layer, the coordinate covalent bonds (Ni–Cl) of $[NiCl_4]^{2-}$ were broken, and then the re-free Cl^- (Cl in the broken Ni–Cl bonds) moved against the cathode while the re-free Ni^{2+} (Ni in the broken Ni–Cl bonds) moved towards the cathode. Re-free Ni^{2+} moved in parallel over the cathode and chose the easiest place to attach, usually at the defects and at the steps, for the electrodeposition growth of Ni. Defects (normally, cavate

defects and bulging defects) would inevitably occur during the 2D growth of Ni on the cathode, transformed the growth from 2D to 3D (the effects of defects on flat growth was not considered here, but considered the effects on the z-axis direction growth). Ideally, the chances of a new layer growing in each direction caused by a single defect were the same, in other words, the new layer should grow outward in a circular shape (the effects of defects on z-axis direction growth was not considered here, but considered the effects on the flat growth). However, what we saw from Fig. 2 b_2 and c_2 were pyramids rather than circular cones, because the growth of a new layer was still accompanied by a large number of defects that appeared at the frontiers of growth; each defect would make its state differ slightly from the surrounding growth frontiers (a very small range); thus, the resulted Ni nanocone was strictly an *N*-sided polygonal pyramid, which was called local disorder. Although there were different statuses (growth rate, growth direction, etc.) between two adjacent defects, it was negligible compared to those two defect aggregation points that were far apart. At the macro level, only two defect aggregation points with sufficient status differences that
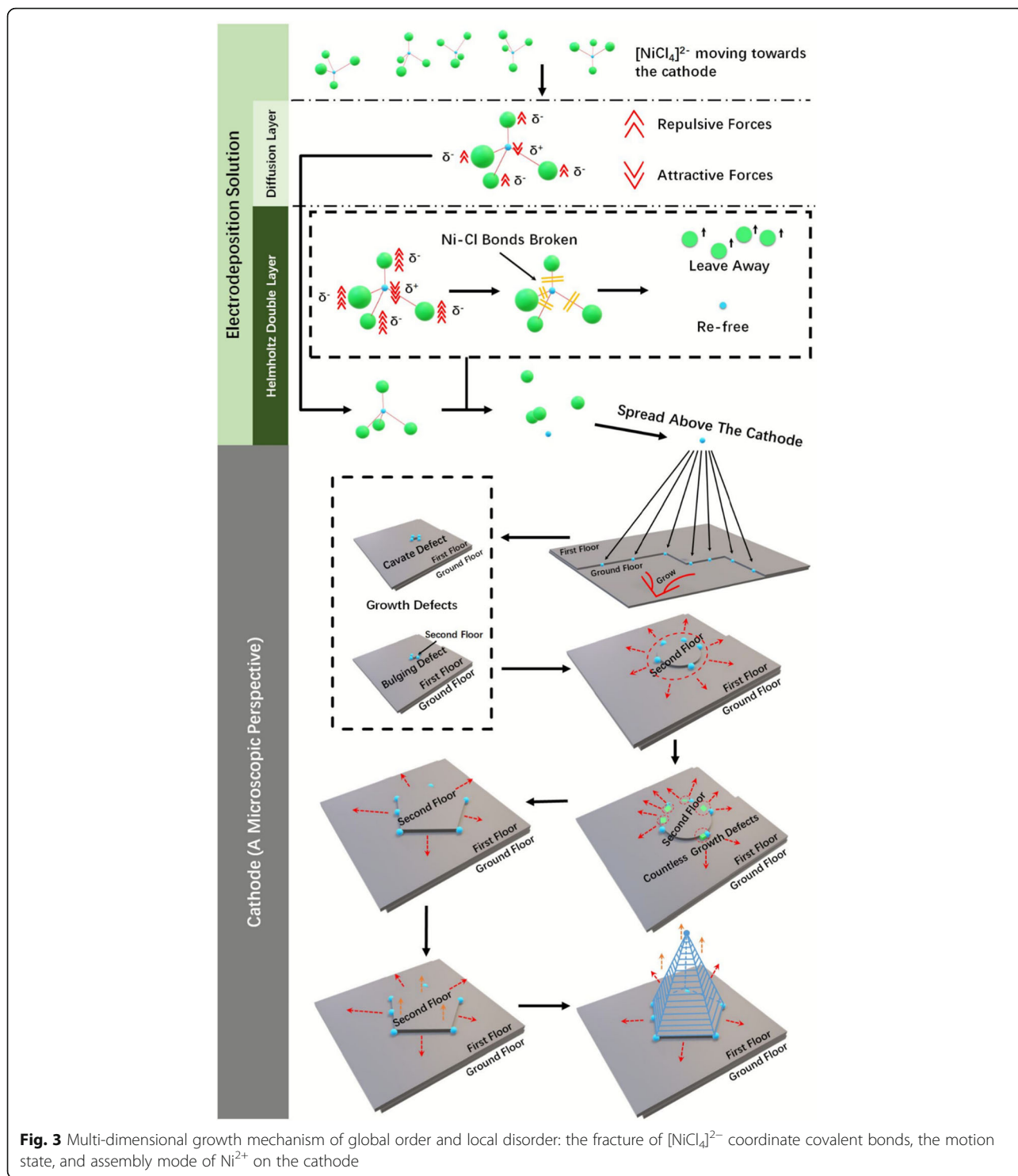
Fig. 3 Multi-dimensional growth mechanism of global order and local disorder: the fracture of $[NiCl_4]^{2-}$ coordinate covalent bonds, the motion state, and assembly mode of Ni^{2+} on the cathode

deserved attention and isolated defects within certain statuses ranges were "merged," Ni nanocones we observed shown a pyramid (triangular, quadrangular, pentagonal, hexagonal pyramid, etc.), which was called global order (Fig. S1).

Effect of Components

In order to further study the specific effect of components in the solution, control variates were used to make preliminary analysis of the surface nanostructure obtained by electrodeposition at different concentrations of

NaCl, $NiCl_2$, and H_3BO_3, respectively, and draw corresponding conclusions.
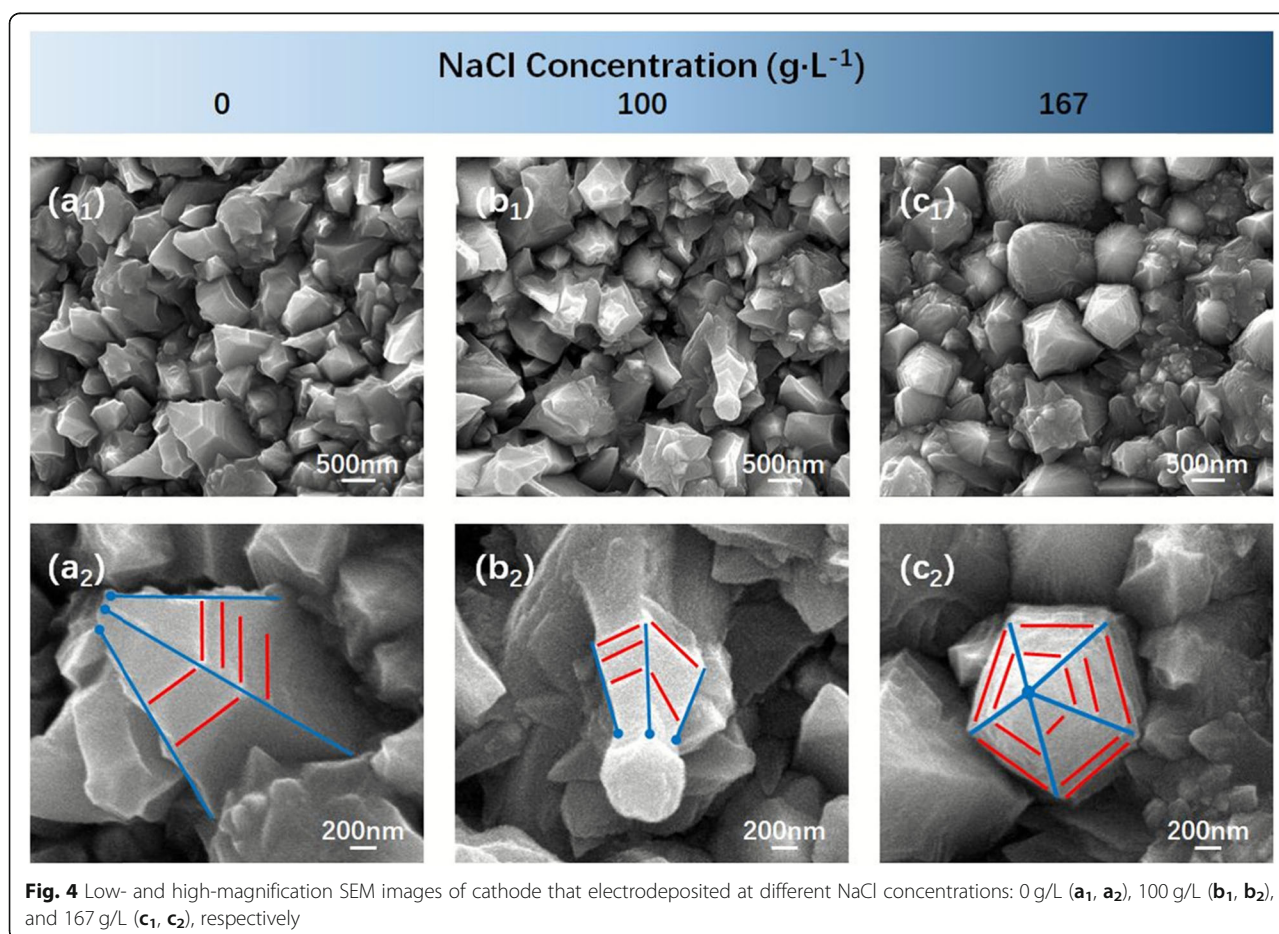
Effect of NaCl

Figure 4 shows the low- and high-magnification SEM images of cathode that electrodeposited under different NaCl concentrations at 0 g/L (Fig. 4 a_1 and a_2), 100 g/L (Fig. 4 b_1 and b_2) and 167 g/L (Fig. 4c_1 and c_2), respectively. When NaCl was not added to the solution, the cathode surface was covered by blocky Ni_{270} nanostructure (Fig. 4 a_1), and although some blocks had a spire-shaped tendency at the apex (Fig. 4a_2), it seemed to be just called undeveloped Ni_{270} nanocones. The reason why it resulted in a large number of undeveloped Ni nanocones on the surface of the cathode was that only $NiCl_2$ in the solution provided Cl^-, which made too less Cl^- to produce a large number of $[NiCl_4]^{2-}$, and further seriously hindered the generation of Ni_{270} nanocones. When the concentration of NaCl increased (100 g/L), it could be observed that there were still some undeveloped Ni_{370} nanocones (Fig. 4 b_1), but a more pronounced trend of Ni nanocones in some places (Fig. 4b_2). This was because the addition of NaCl in the solution greatly alleviated the lack of Cl^-, promoted the

formation of $[NiCl_4]^{2-}$, but it still could not reach a ratio of 1:4 ($n(Ni^{2+}):n(Cl^-)$), and the cathode surface was covered by many undeveloped Ni_{370} nanocones. Continuing to increase the concentration of NaCl to 167 g/L, it could be found that most of the cathode surface was covered by Ni_{437} nanocones which made it almost impossible to detect undeveloped Ni_{437} nanocones (Fig. 4 c_1, c_2). The large amount of Cl^- in the solution made it possible to produce huge number of $[NiCl_4]^{2-}$, which greatly promoted the generation of electrodeposited Ni_{437} nanocones.

Effect of $NiCl_2$

Figure 5 shows the low- and high-magnification SEM images of cathode that electrodeposited under different $NiCl_2$ concentrations: 0 g/L (Fig. 5 a_1 and a_2), 200 g/L (Fig. 5 b_1 and b_2), 400 g/L (Fig. 5 c_1 and c_2), respectively. It was clear from Fig. 5 a_1 that the cathode surface was covered by a cotton floc-shaped structure, and the entire surface structure tended to be more densely stacked with Ni balls but no cones structure (Fig. 5a_2). The reason why Ni^{2+} electrodeposited on the cathode in a slow and more average way and caused a cotton floc-shaped structure was that there was no Ni^{2+} in the solution before
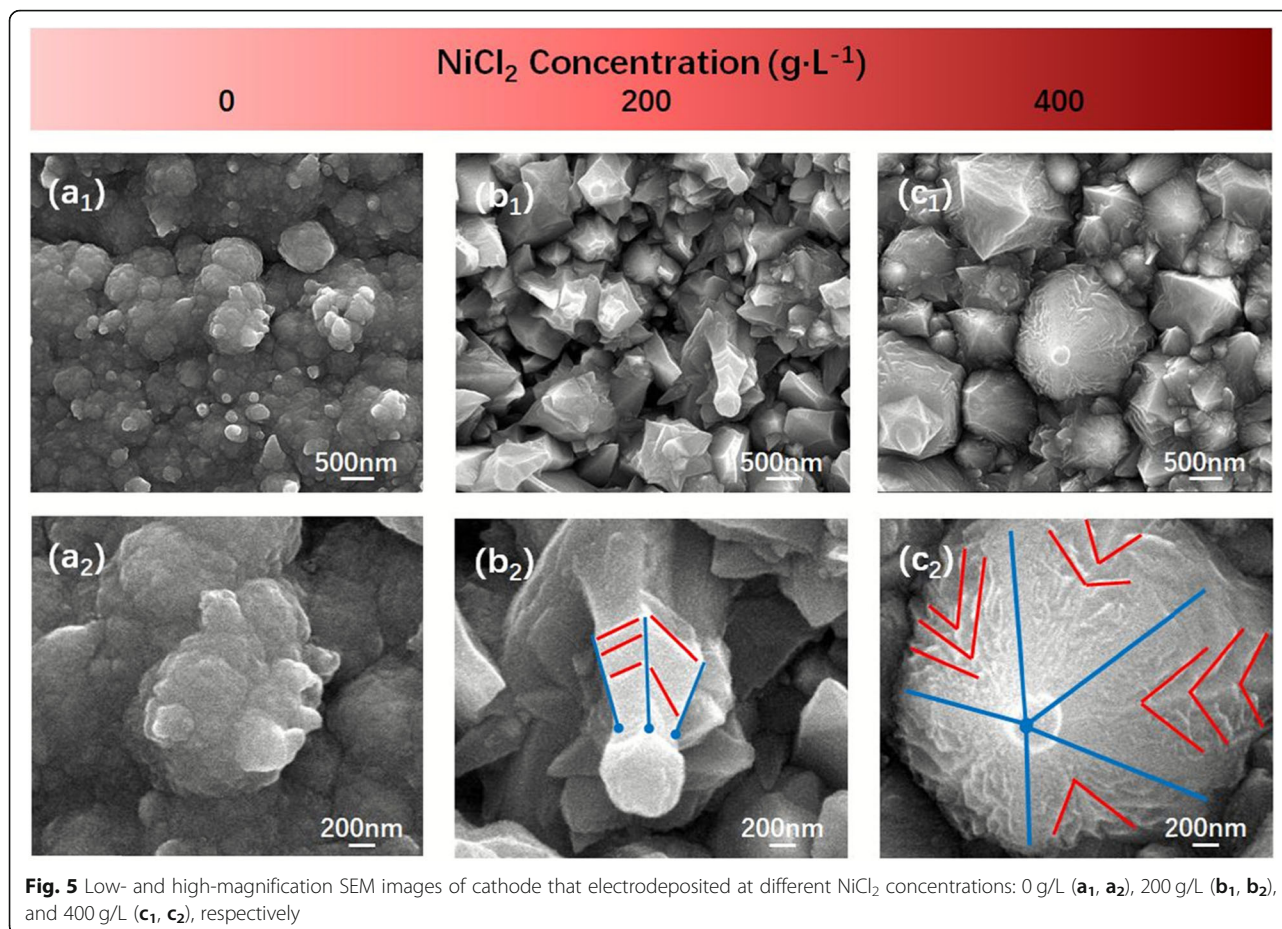

Fig. 4 Low- and high-magnification SEM images of cathode that electrodeposited at different NaCl concentrations: 0 g/L (**a₁**, **a₂**), 100 g/L (**b₁**, **b₂**), and 167 g/L (**c₁**, **c₂**), respectively

Fig. 5 Low- and high-magnification SEM images of cathode that electrodeposited at different $NiCl_2$ concentrations: 0 g/L (**a_1**, **a_2**), 200 g/L (**b_1**, **b_2**), and 400 g/L (**c_1**, **c_2**), respectively

electrodeposition; Ni^{2+} required for electrodeposition all came from those Ni atoms which lost electrons on the anode, resulting in low concentration of Ni^{2+} in the solution, so even if there were a large number of Cl^-, the generation of $[NiCl_4]^{2-}$ was rare, which seriously hindered the formation of Ni nanocones structure. After increasing the concentration of $NiCl_2$ in the solution to 200 g/L, the electrodeposited cathode surface was covered by some Ni_{370} nanocones and others undeveloped (Fig. 5 b_1), the entire surface was rough and fragmented (Fig. 5b_2). $NiCl_2$ added to the solution greatly increased the generation of $[NiCl_4]^{2-}$, prompted the formation of Ni_{370} nanocones, but a part of underdeveloped Ni_{370} nanocones indicated that the concentration might not have reached the optimal level. When the concentration of $NiCl_2$ reached 400 g/L, the cathode surface was covered by a large number of huge Ni_{570} nanocones (Fig. 5 c_1), some of them presented vaguely visible edges but more conical shapes, and the cone surface was full of texture, with sharp angles and tips pointed to the cone vertex (Fig. 5 c_2, red lines). Theoretically, the concentration of Ni^{2+} provided by $NiCl_2$ (400 g/L) was far greater than that desired, which instead highlighted the lack of Cl^-; then, a large number of Ni^{2+} electrodeposited on the cathode during a short period of time resulted in Ni_{570}

nanocones grown too fast to present the local disorder characteristics but emerged cone structure.

Effect of H_3BO_3

In the series of experiments, H_3BO_3 was the role of pH regulator, since boron (B) was an electron-deficient atom, it could combine with hydrogen oxygen root ions (OH^-) from the water molecules, and thereby release hydrogen ions (H^+) (Eq. 1).
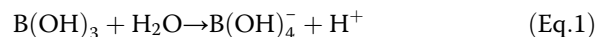
$$B(OH)_3 + H_2O \rightarrow B(OH)_4^- + H^+ \qquad (Eq.1)$$

Figure 6 shows the low- and high-magnification SEM images of cathode that electrodeposited from different H_3BO_3 concentrations: 0 g/L (Fig. 6 a_1 and a_2), 25 g/L (Fig. 6 b_1 and b_2), 50 g/L ((Fig. 6c_1 and c_2), respectively. In Fig. 6a_1, it could be clearly seen that the cathode was covered with a relatively flat electrodeposition layer, and some areas had slight protrusions (Fig. 6 a_2), but no Ni_{320} nanocones structure overall. When there was no H_3BO_3 in the solution, only electrolyzed water reaction would occur near the cathode, so the solution was generally in an acid-base equilibrium state, and Ni^{2+} were almost immune to the influence of OH^- or H^+, resulting in a flat
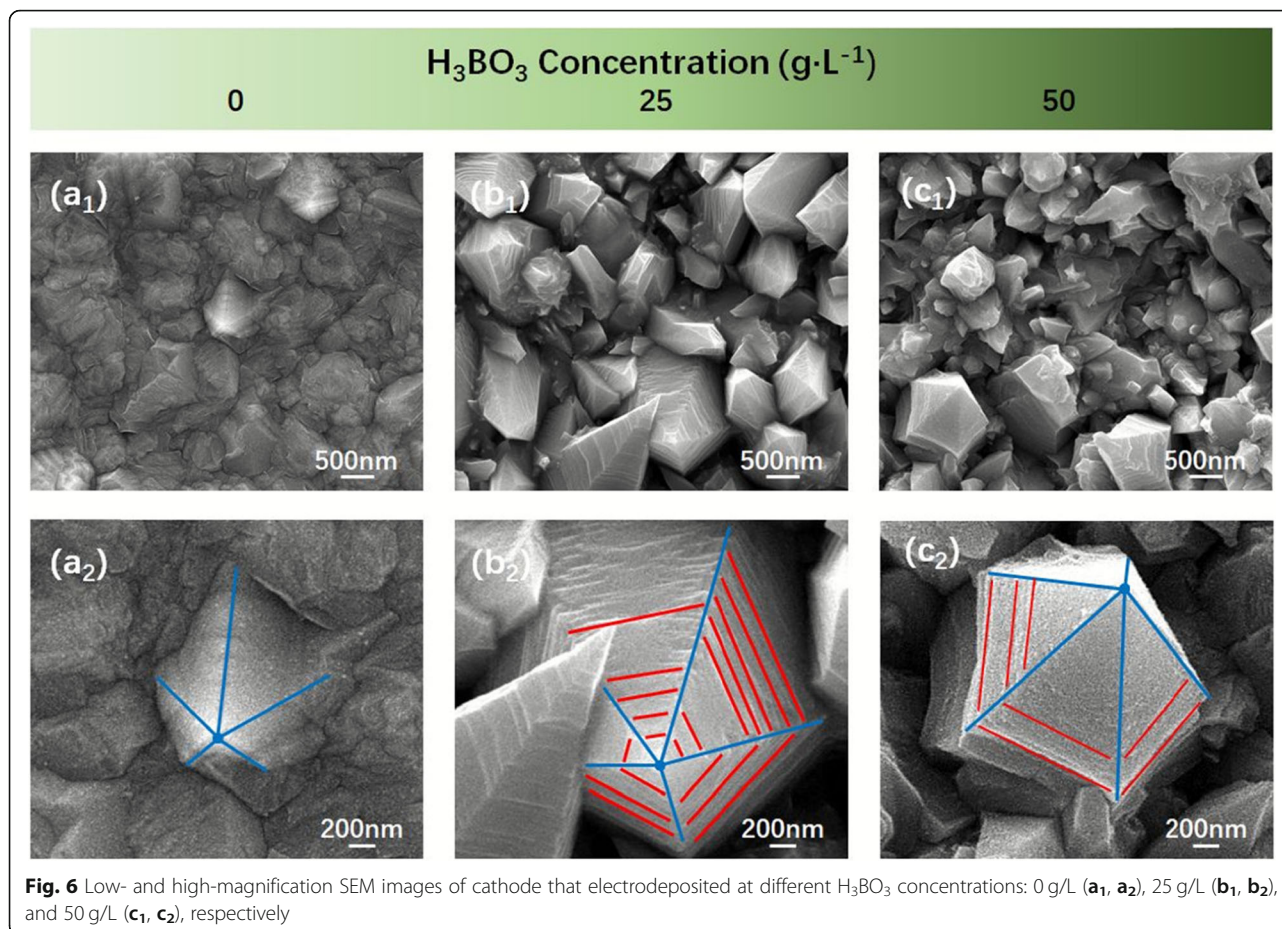
Fig. 6 Low- and high-magnification SEM images of cathode that electrodeposited at different H_3BO_3 concentrations: 0 g/L (**a$_1$**, **a$_2$**), 25 g/L (**b$_1$**, **b$_2$**), and 50 g/L (**c$_1$**, **c$_2$**), respectively

electrodeposition layer. Adding H_3BO_3 to 25 g/L in the solution, we could observe obvious huge Ni_{345} nanocones structure from Fig. 6 b$_1$, while the texture trend was complex, the edges and corners were clear (Fig. 6b$_2$). This was due to the addition of H_3BO_3, which supplied more H^+ near the cathode, resulting in a weak acidity environment. When the concentration of H_3BO_3 in the solution reached 50 g/L, the size of Ni_{370} nanocone was reduced, compared to Ni_{345} nanocones, but the surface texture was smoother. This was due to the large number of H_3BO_3, which made the solution appear weak acidic (slightly more acidic than the previous one), the excessive H^+ affected the size of Ni_{370} nanocones but made the surface more regular.

Overall, the size of Ni nanocones was not proportional relationship to the amount of H_3BO_3 in the solution. This might be that when the solution was free of H_3BO_3, the negatively charged OH^- interfered with the positive electricality Ni^{2+}, which affected the motion of Ni^{2+}. On another hand, when a large amount of H_3BO_3 was presented in the solution, a lot of H^+ would attach the cathode surface to generate hydrogen (H_2), but due to the small size of H^+ itself, the influence on the nanostructure of Ni nanocones was quite limited.

Conclusion

In summary, we had successfully synthesized Ni nanocones via electrodeposition process in the solution containing $NiCl_2$, $NaCl$, and H_3BO_3. The results have shown that the intermediate product was a special complex, which still presented after the reaction and had poor high-temperature resistance, and that Ni nanocones were pure Ni with fcc structure, grown mainly along (220) crystal face. Moreover, the specific structure of the intermediate product was supported by known mature theoretical systems, the nanostructure and electrodeposition process of the products were investigated, and the probable formation mechanism of Ni nanocones was discussed based on the experimental results. Meanwhile, we found that the nanostructure of Ni nanocones could be controlled by adjusting the experimental conditions such as the concentration of $NiCl_2$, $NaCl$, and H_3BO_3, respectively. Therefore, establishing appropriate parameters was key point for the synthesis of Ni crystals with nanocones structure via this electrodeposition approach. Additionally, we expected that this novel strategy could be possibly extended to some other magnetic metals to synthesize controllable nanocone structure.

Zou *et al. Nanoscale Research Letters* (2020) 15:91

Page 9 of 10

Supplementary information

> **Additional file 1:. Figure S1.** The supplementary of multi-dimensional growth mechanism of global order and local disorder

Authors' Contributions
RZ and JW conceived and designed the experiments. SX and LG performed the experiments and analyzed the data. YL and YW helped in interpretation and discussions. RZ and JW wrote the manuscript. All authors read and approved the final manuscript.

Availability of Data and Materials
The datasets used for supporting the conclusion are included in the article and the supporting file.

Competing Interests
The authors declare that they have no competing interests.

Author details
[1]School of Materials Science and Engineering, Xihua University, Chengdu 610039, People's Republic of China. [2]School of Automotive Engineering, Chongqing University, Chongqing 400044, People's Republic of China. [3]School of Optoelectronic Science and Engineering & Collaborative Innovation Center of Suzhou Nano Science and Technology, Soochow University, Suzhou 215006, People's Republic of China.

References
1. Gleiter H (2000) Nanostructured materials: basic concepts and microstructure. Acta Mater 48(1):1–29
2. Lee ML, Jung KK, Lee SH, Ko JS (2016) One-step fabrication of nickel nanocones by electrodeposition using CaCl$_2$·2H$_2$O as capping reagent. Appl Surf Sci 369:163–169
3. Hönes R, Ruhe J (2018) "Nickel Nanoflowers" with surface-attached fluoropolymer networks by C,H insertion for the generation of metallic superhydrophobic surfaces. Langmuir 34:1–36
4. Salehikahrizsangi P, Raeissi K, Karimzadeh F, Calabrese L, Patane S, Proverbio E (2018) Erosion-corrosion behavior of highly hydrophobic hierarchical nickel coatings. Colloid Surface A 558:446–454
5. Xiang T, Chen D, Lv Z, Yang Z, Yang L, Li C (2019) Robust superhydrophobic coating with superior corrosion resistance. J Alloys Compd 798:320–325
6. Gao S, Sui Y, Wei F, Qi J, Meng Q, Ren Y, He Y (2018) Dandelion-like nickel/cobalt metal-organic framework based electrode materials for high performance supercapacitors. J Colloid Interface Sci 531:83–90
7. Yoon Y, Kim D, Lee J-B (2014) Hierarchical micro/nano structures for super-hydrophobic surfaces and super-lyophobic surface against liquid metal. Micro Nano Syst Lett 2:3
8. Lee JM, Lee SH, Ko JS (2015) Influence of open area ratio on microstructure shape in Cu–Ni alloy electrodeposition. Appl Phys A Mater Sci Process 118:579–585
9. Zhou Y, Sreekala S, Ajayan PM, Nayak SK (2008) Resistance of copper nanowires and comparison with carbon nanotube bundles for interconnect applications using first principles calculations. J Phys-Condens Mat 20:095209
10. Wang J, Yang F, Wei X, Zhang Y, Wei L, Zhang J, Tang Q, Guo B, Xu L (2014) Controlled growth of conical nickel oxide nanocrystals and their high performance gas sensing devices for ammonia molecule detection. Phys Chem Chem Phys 16:16711–16718
11. Wang J, Yang P, Wei X (2015) High-performance, room-temperature, and no-humidity-impact ammonia sensor based on heterogeneous nickel oxide and zinc oxide nanocrystals. ACS Appl Mater Interfaces 7(6):3816–3824
12. Ye J, Gagliardi L, Cristopher JC, Truhlar DG (2017) Single Ni atoms and Ni$_4$ clusters have similar catalytic activity for ethylene dimerization. J Catal 354:278–286
13. Budi CS, Saikia D, Chen C-S, Kao H-M (2019) Catalytic evaluation of tunable Ni nanoparticles embedded in organic functionalized 2D and 3D ordered mesoporous silicas from the hydrogenation of nitroarenes. J Catal 370:274–288
14. Wang Y, Zhu Y, Liu Z, Wang L, Xu D, Fang C, Wang S (2019) Catalytic performances of Ni-based catalysts on supercritical water gasification of phenol solution and coal-gasification wastewater. Int J Hydrogen Energ 44(7):3470–3480
15. Li M, van Veen AC (2018) Tuning the catalytic performance of Ni-catalysed dry reforming of methane and carbon deposition via Ni-CeO$_{2-x}$ interaction. Appl Catal B-Environ 237:641–648
16. Gong W, Jiang Z, Wu R, Liu Y, Huang L, Hu N, Tsiakaras P, Shen PK (2019) Cross-double dumbbell-like Pt–Ni nanostructures with enhanced catalytic performance toward the reactions of oxygen reduction and methanol oxidation. Appl Catal B-Environ 246:277–283
17. Hassani KE, Kalnina D, Turks M, Beakou BH, Anouar A (2019) Enhanced degradation of an azo dye by catalytic ozonation over Ni-containing layered double hydroxide nanocatalyst. Sep Purif Technol 210:764–774
18. Xie X, Chen M, Liu P, Shang J, Liu T (2018) Synergistic catalytic effects of the Ni and V nanoparticles on the hydrogen storage properties of Mg-Ni-V nanocomposite. Chem Eng J 347:145–155
19. Long H, Liu X, Xie Y, Hu N, Deng Z, Jiang Y, Wei Q, Yu Z, Zhang S (2019) Thickness effects of Ni on the modified boron doped diamond by thermal catalytic etching for non-enzymatic glucose sensing. Electroanal Chem 832:353–360
20. Zhang Z, Cui J, Zhang J, Liu D, Yu Z, Guo D (2019) Environment friendly chemical mechanical polishing of copper. Appl Surf Sci 467-468:5–11
21. Zhang Z, Wang B, Kang R, Zhang B, Guo D (2015) Changes in surface layer of silicon wafers from diamond scratching. CIRP Ann-Manuf Techn 64(1):394–352
22. Wang B, Zhang Z, Chang K, Cui J, Rosenkranz A, Yu J, Lin C-T, Chen G, Zang K, Luo J, Jiang N, Guo D (2018) New deformation-induced nanostructure in silicon. Nano Lett 18:4611–4617
23. Cui J, Zhang Z, Liu D, Zhang D, Hu W, Zou L, Lu Y, Zhang C, Lu H, Tang C (2019) Unprecedented piezoresistance coefficient in strained silicon carbide. Nano Lett 19:6569–6576
24. Jafari A, Jahromi SP, Boustani K, Goh BT, Huang NM (2019) Evolution of structural and magnetic properties of nickel oxide nanoparticles: influence of annealing ambient and temperature. J Magn Magn Mater 469:383–390
25. Fa D, Yu B, Miao Y (2019) Synthesis of ultra-long nanowires of nickel phosphate by a template-free hydrothermal method for electrocatalytic oxidation of glucose. Colloid Surface A 564:31–38
26. Zanganeh N, Rajabi A, Torabi M, Allahkarami M, Moghaddas A, Sadrnezhaad SK (2014) Growth and microstructural investigation of multiwall carbon nanotubes fabricated using electrodeposited nickel nanodeposits and chemical vapor deposition method. J Mol Struct 1074:250–254
27. Mehrabi M, Reyhani A, Parvin P, Mortazavi SZ (2019) Surface structural alteration of multi-walled carbon nanotubes decorated by nickel nanoparticles based on laser ablation/chemical reduction methods to enhance hydrogen storage properties. Int J Hydrogen Energ 44(7):3812–3823
28. Ni X-M, Su X-B, Yang Z-P, Zheng H-G (2003) The preparation of nickel nanorods in water-in-oil microemulsion. J Cryst Growth 252(4):612–617
29. Wang Y, Zhu Q, Zhang H (2007) Selected-control synthesis of hierarchical nickel structures. Mater Res Bull 42(8):1450–1456
30. Rahimi E, Davoodi A, Rashid ARK (2018) Characterization of screw dislocation-driven growth in nickel micro-nanostructure electrodeposition process by AFM. Mater Lett 210:341–344
31. Geng W, Hu A, Li M (2012) Super-hydrophilicity to super-hydrophobicity transition of a surface with Ni micro–nano cones array. Appl Surf Sci 263:821–824

32. Rahimi E, Rafsanjani-Abbasi A, Imani A, Rashid ARK, Hosseinpour S, Davoodi A (2019) Synergistic effect of a crystal modifier and screw dislocation step defects on the formation mechanism of nickel micro-nanocone. Mater Lett 245:68–72

33. Wang N, Hang T, Shanmugam S, Li M (2014) Preparation and characterization of nickel-cobalt alloy nanostructures array fabricated by electrodeposition. CrystEngComm 16:6937–6943

34. Pathak DK, Chaudhary A, Mishra S, Yogi P, Saxena SK, Sagdeo PR, Kumar R (2019) Precursor concentration dependent hydrothermal NiO nanopetals: Tuning morphology for efficient applications. Superlattice Microst 125:138–143

35. Lee JM, Jung KK, Ko JS (2016) Effect of NaCl in a nickel electrodeposition on the formation of nickel nanostructure. J Mater Sci 51:3036–3044

36. Hashemzadeh M, Raeissi K, Ashrafizadeh F, Khorsand S (2015) Effect of ammonium chloride on microstructure, super-hydrophobicity and corrosion resistance of nickel coatings. Surf Coat Technol 283:318–328

37. Chinnappan A, Kim H (2012) Nanocatalyst: Electrospun nanofibers of PVDF-Dicationic tetrachloronickelate (II) anion and their effect on hydrogen generation from the hydrolysis of sodium borohydride. Int J Hydrogen Energ 37(24):18851–18859

38. Fernandes LC, Correia DM, García-Astrain C, Pereira N, Tariq M, Esperança JMSS, Lanceros-Méndez S (2019) Ionic-liquid-based printable materials for thermochromic and thermoresistive applications. ACS Appl Mater Interfaces 11(22):20316–20324

Publisher's Note